



Computer Methods in Biomechanics and Biomedical Engineering: Imaging & Visualization

ISSN: (Print) (Online) Journal homepage: <https://www.tandfonline.com/loi/tciv20>

The hip joint as an egg shape: a comprehensive study of femoral and acetabular morphologies

Daniel Simões Lopes, Sara M. Pires, Carolina D. Barata, Vasco V. Mascarenhas & Joaquim A. Jorge

To cite this article: Daniel Simões Lopes, Sara M. Pires, Carolina D. Barata, Vasco V. Mascarenhas & Joaquim A. Jorge (2020) The hip joint as an egg shape: a comprehensive study of femoral and acetabular morphologies, *Computer Methods in Biomechanics and Biomedical Engineering: Imaging & Visualization*, 8:4, 411-425, DOI: [10.1080/21681163.2019.1709902](https://doi.org/10.1080/21681163.2019.1709902)

To link to this article: <https://doi.org/10.1080/21681163.2019.1709902>



Published online: 08 Jan 2020.



Submit your article to this journal [↗](#)



Article views: 104






View related articles [↗](#)



View Crossmark data [↗](#)



The hip joint as an egg shape: a comprehensive study of femoral and acetabular morphologies

Daniel Simões Lopes ^{a,b}, Sara M. Pires^{a,b}, Carolina D. Barata^{a,b}, Vasco V. Mascarenhas ^c and Joaquim A. Jorge ^{a,b}

^aINESC-ID Lisboa, Lisboa, Portugal; ^bInstituto Superior Técnico, Universidade de Lisboa, Lisboa, Portugal; ^cHospital da Luz, UIIME, Lisboa, Portugal

ABSTRACT

Understanding the morphological features characterising a normal femoral head and acetabular cavity is critical for a more comprehensive and updated definition of hip anatomy. Based on anatomical observations, MacConaill introduced the notion that spheroidal articular surfaces are better represented by ovoidal shapes, in comparison with the still well-established spherical shape. This work tests MacConaill's classification by using a surface-fitting framework to assess the goodness-of-fit regarding the largest assortment of sphere-like shapes presented in a single study (i.e. a total of 10 different shapes: sphere, rotational conchoids, rotational ellipsoid, ellipsoid, superellipsoid, Barr's superellipsoid, tapered ellipsoid, Barr's tapered superellipsoid, ovoid, superovoid). Anatomical data of the femoral head and acetabular cavity were obtained from computed tomography scans of a gender-balanced, asymptomatic 15 population of 30 adult subjects. The framework involved image segmentation with active contour methods, mesh smoothing and decimation, and surface fitting to point clouds was performed with genetic algorithms. The statistical analysis of the surface-fitting errors revealed the superior approximation of non-spherical shapes: superovoids provided the best fit for each femoral head and acetabular cavity, whereas spheres presented the worst fitting values. We also addressed gender variability in bony 20 hip geometry as sphericity, ellipticity, conicity and squareness were measured.

ARTICLE HISTORY

Received 29 April 2019
Accepted 24 December 2019

KEYWORDS

Femoral head; acetabular cavity; implicit surfaces; surface fitting; sphere; ovoid

1. Introduction

The morphology of the hip joint has been a topic of interest for anatomists and physicians during many centuries (Vesalius 1998). Given its influence on the effective and efficient performance of daily physical activities, the orthopaedic community has also put a great emphasis on hip joint morphology to better understand bone geometry in asymptomatic conditions, as normal hip characterisation helps clarify the distinctive morphological features when compared to pathological deformities, such as femoroacetabular impingement and hip dysplasia (Lopes et al. 2018). Moreover, understanding the morphology of the femoral head and acetabular cavity may even inspire new prosthetic devices as form is intimately related to biomechanical joint function.

According to the standard classification of synovial joints (Rouvière et al. 2005), the hip articulation falls under the classification of spheroidal joints given its visual similarities to a sphere or a hemisphere. In fact, the articular surfaces of this joint (i.e. femoral head and acetabular cavity) were regarded as being best represented by the spherical shape for a considerable amount of time, and this view has not yet fallen completely in disuse (Rouvière et al. 2005; Williams et al. 2010). Nevertheless, there have been studies contradicting this belief (MacConaill 1966, 1973; Menschik 1997; Kang 2004; Kang et al. 2010; Standing 2015; Lopes et al. 2018). It has long been suggested that the articular surfaces of asymptomatic hip joints are only symmetric in a limited number of axes, presenting an egg-like or

ovoidal shape instead of a spherical one. Attributing an egg shape to a synovial joint is known as MacConaill's ovoidal joint classification (MacConaill 1966, 1973; Standing 2015).

To assess the veracity of this classification, several authors have conducted studies on the morphological features of articular surfaces by approximating spheres (S), rotational conchoids (RC), and ellipsoids (E) to the femoral head and/or the acetabular cavity (Menschik 1997; Xi et al. 2003; Kang 2004; Kang et al. 2010; Anderson et al. 2010; Subburaj et al. 2010; Berryman et al. 2014; Cerveri et al. 2014). Studies on prosthetic designs for the femoral head were also carried out (Jiang et al. 2010; Liu et al. 2014, 2015), in which the artificial articular surface was approximated by an ellipsoidal shape. Besides these shapes, rotational ellipsoids (RE) have also been considered as an approximated surface (Gu et al. 2008, 2010, 2011; Cerveri et al. 2011; Wu et al. 2016). However, these shapes do not satisfy MacConaill's classification as they do not account for essential ovoid characteristics, namely, axial asymmetry and non-homogeneous curvature (Carter 1968; Paganelli et al. 1974; Todd and Smart 1984). To this end, Lopes et al. (2015) computationally tested the ovoid conjecture for the femoral head by performing a shape analysis that compared spheres and ellipsoids against superellipsoids (SE), ovoids (O) and superovoids (SO), while a more recent work studied the shape of asymptomatic, dysplastic and impinged hip joints by comparing spheres, ellipsoids and tapered ellipsoids (TE) (Lopes et al. 2018). (Table 1) summarises surface-fitting results of several

papers on shape analysis of femoral head and acetabular cavity surfaces.

Despite the amount of work reported in the literature, to the authors' knowledge, there still lacks a thorough and exhaustive comparison between a wider variety of shapes that resemble and better represent hip joint reconstructions taken from CT data-sets. In this paper, we aim to better evaluate the limit of hip joint sphericity by comparing 10 different shapes through a robust surface-fitting framework, and by measuring egg shape features such as ellipticity and conicity. We also introduce as a third shape feature, squareness, as supra-quadratic shapes have indicated better results when compared to spheres and ellipsoids (Lopes et al. 2015). In addition, it is well known that the bony geometry of the pelvis is complex and that gender differences exist. While multiple studies have catalogued these differences, most of the measurements are not directly related to ellipticity or conicity, much less to squareness. In line with MacConaill's classification, we hypothesised that gender differences existed in terms of ellipticity and conicity of the articular surfaces of the hip joint.

Therefore, the major goals of this work are to address the following morphological questions: (i) how aspherical are the

femoral heads and acetabular cavities of healthy hip joints when compared to ellipsoidal and ovoidal shapes? (ii) which shape primitive can be considered the most representative of a healthy hip joint? (iii) how does sphericity, ellipticity, conicity and squareness vary among sexes? and (iv) can we identify morphological similarities between genders? Therefore, this work intends to carry on previous research on hip joint morphology (Lopes et al. 2015, 2018) by convening, in a single paper, the shape analyses of femoral heads and acetabular cavities of asymptomatic hips. Such a comprehensive study compares a broad spectrum of shape primitives either reported in the literature (e.g. sphere, rotational conchoid, rotational ellipsoid, ellipsoid, superellipsoid, ovoid, superovoid) or newly introduced shapes (e.g. Barr's superellipsoids (SEB), tapered ellipsoids (TE) and Barr's tapered superellipsoids (TSEB)). In order to address which shape primitive best portrays the morphological features of a normal hip joint, an optimisation scheme was developed to compute the signed Euclidean distances between each point in the reconstructed 3D scan and the optimally fitted shapes. Error-of-fit statistical analyses were then performed to sort out the best and worst shapes. Finally, the shape features to describe sphericity, ellipticity, conicity and squareness are compared between both sexes.

Table 1. Summary of studies regarding the surface fitting of geometric primitives onto spheroidal articular surfaces of the hip joint. (FH – femoral head; AC – acetabular cavity; S – sphere; RE – rotational ellipsoid; E – ellipsoid; SE – superellipsoid; O – ovoid; SO – superovoid; RC – rotational conchoid).

Author(s) (year)	Population size	Anatomical structure	Geometric primitives	Surface fitting error (mm)		
				Mean μ	RMS	
Menschik (1997)	10	FH	S	-	0.155 (min)	
			RC	-	0.148 (min)	
		AC	S	-	0.187 (min)	
Xi et al. (2003)	12	AC	RC	-	0.152 (min)	
			S	Male	Female	-
			RC	0.39	0.50	-
			E	0.43	0.53	-
Gu et al. (2008)	25	AC	S	0.29	0.38	-
			RE	0.498	-	
Anderson et al. (2010)	1	FH	S	0.446	-	
			RC	0.182	-	
		AC	S	0.531	-	
Gu et al. (2010)	25	AC	RC	0.172	-	
			S	0.530	-	
			RE	0.423	-	
Cerveri et al. (2011)	20	AC	S	0.496	-	
			E	-	1.6	
Gu et al. (2011)	2	FH	S	Male	Female	-
			RE	0.374	0.404	-
		AC	S	0.348	0.373	-
		RE	0.434	0.656	-	
Cerveri et al. (2014)	11	AC	RE	0.398	0.590	-
			S	1.95	-	
			RC	1.28	-	
Berryman et al. (2014)	44	FH	E	1.14	-	
			S	-	1.2	
Lopes et al. (2015)	11	FH	S	0.643	-	
			E	0.544	-	
			SE	0.532	-	
			O	0.484	-	
			SO	0.493	-	
			S	0.653	-	
Lopes et al. (2018)	20	FH	E	0.789	-	
			TE	0.653	-	
			S	0.789	-	
		AC	S	0.789	-	
			E	0.653	-	
			TE	0.789	-	

2. Material and methods

The image-based anatomical workflow followed the pipeline presented in work previously carried out by Lopes et al. (2015) (Figure 1). CT data sets of asymptomatic hip joints were used to extract the geometric information necessary for 3-D reconstruction. Semi-automatic segmentation techniques were used to extract the anatomical information. In order to guarantee homogeneous nodal distribution and attenuate artefacts resulting from model creation, mesh adjustment operations such as smoothing and decimation filters were applied to the reconstructed models. From the 3-D models, only the regions corresponding to the articulating surfaces are of interest and were manually selected and stored as point clouds. A surface-fitting tool was then used to adjust 10 different smooth convex shapes, using a genetic algorithm to solve a non-linear least-squares minimisation problem, to the point clouds of femoral heads and acetabular cavities of 30 subjects. Here, surface fitting is formulated as a minimisation problem in which the objective function is highly non-linear presenting a large number of local minima. Standard optimisation algorithms are not well suited for such minimisation problems (Bazaraa et al. 1993). A genetic algorithm was considered as it

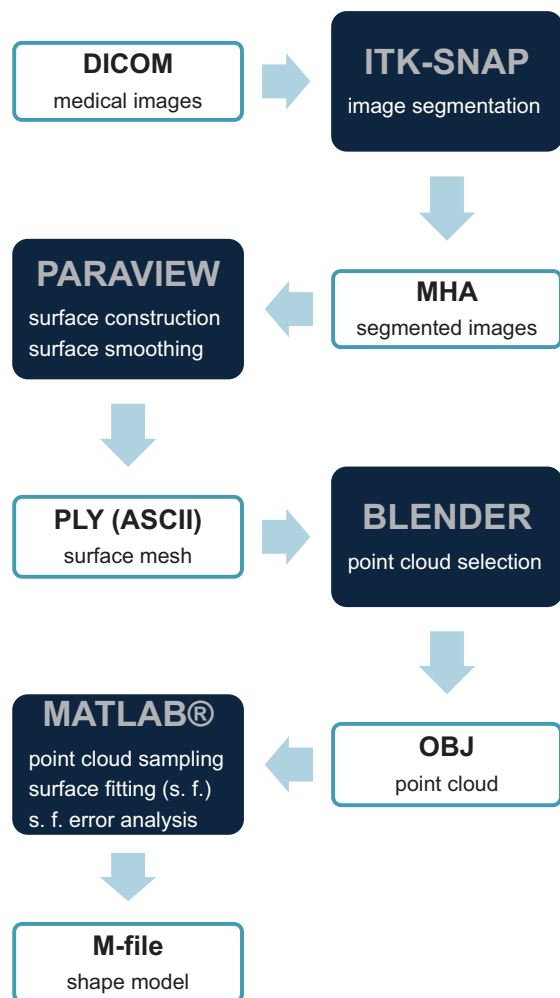


Figure 1. Sequence of computational applications used for anatomical and geometric information extraction and modelling of spheroidal articular surfaces of the hip joint. White boxes represent the file formats used as input in the software tools referenced in the blue boxes.

consists of a powerful tool to find optimal solutions for highly non-linear surface-fitting problems (Ahn 2004). Finally, statistical analyses were performed to compare the goodness-of-fit between different shape models that best characterise the articular surfaces of the hip joint in normal conditions.

2.1 Hierarchy of shape models

The macroscopic features of the articular surfaces of the hip joint can be considered as spheroidal, convex, limited, closed, topologically similar to a sphere, and present second-degree continuity for most of the surface range. The chosen geometric primitives do, in fact, display these properties (with the exception of the rotational conchoids which are slightly concave at one end). The considered mathematical models are drawn from previous studies (Barr 1981; Todd and Smart 1984; Menschik 1997) and consist of the following 10 shapes: sphere (S), rotational conchoid (RC), rotational ellipsoid (RE), ellipsoid (E), superellipsoid (SE), Barr's superellipsoid (SEB), tapered ellipsoid (TE), Barr's tapered superellipsoid (TSEB), ovoid (O) and super-ovoid (SO).

However, it is important to stress the hierarchical connection between all the shape primitives, in order to fully understand how the surface-fitting process is built. Considering the initial and simplest surface represented in (Figure 2), the sphere, it is possible to obtain the remaining surfaces through non-linear morphing operations, such as rescaling, exponentiation and asymmetrisation. The changes generated by these actions are easily identified on the resulting surface, being the higher level of squareness exhibited by surfaces such as superellipsoids, superovoids and tapered superellipsoids an example of the modifications introduced by variation in exponentiation. The orientation of the arrows composing the hierarchical graph (Figure 2) indicates which shape models constitute generalisations and which are particular cases within a given geometric primitive. For example, superovoids are a generalisation of superellipsoids and ovoids, whereas ellipsoids are a particular case of both superellipsoids and tapered ellipsoids.

The implicit surface expressions for all 10 shapes, in the canonical form, are written as

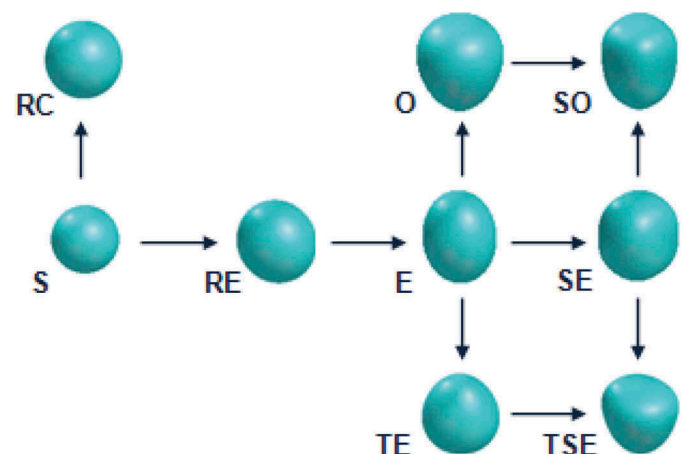


Figure 2. Hierarchical organisation of the different geometric primitives represented in the form of a graph revealing the morphological relationships between the various shapes.

Sphere

$$F_S(x, y, z) = (a^{-1}x)^2 + (a^{-1}y)^2 + (a^{-1}z)^2 \quad (1)$$

Rotationalconchoid

$$F_{RC}(x, y, z) = (x^2 + y^2 + z^2 - ax)^2 - b^2(x^2 + y^2 + z^2) \quad (2)$$

Rotationalellipsoid

$$F_{RE}(x, y, z) = (a^{-1}x)^2 + (b^{-1}y)^2 + (b^{-1}z)^2 \quad (3)$$

Ellipsoid

$$F_E(x, y, z) = (a^{-1}x)^2 + (b^{-1}y)^2 + (c^{-1}z)^2 \quad (4)$$

Superellipsoid

$$F_{SE}(x, y, z) = (a^{-1}x)^{\frac{2}{\epsilon_1}} + (b^{-1}y)^{\frac{2}{\epsilon_2}} + (c^{-1}z)^{\frac{2}{\epsilon_3}} \quad (5)$$

Barr'ssuperellipsoid

$$F_{SEB}(x, y, z) = \left[(a^{-1}x)^{\frac{2}{\epsilon_1}} + (b^{-1}y)^{\frac{2}{\epsilon_1}} \right]^{\frac{\epsilon_1}{\epsilon_2}} + (c^{-1}z)^{\frac{2}{\epsilon_2}} \quad (6)$$

Taperedellipsoid

$$F_{TE}(x, y, z) = \left(\frac{a^{-1}x}{T_x z + 1} \right)^2 + \left(\frac{b^{-1}y}{T_y z + 1} \right)^2 + (c^{-1}z)^2 \quad (7)$$

Barr'staperedsuperellipsoid

$$F_{TSEB}(x, y, z) = \left[\left(\frac{a^{-1}x}{T_x z + 1} \right)^{\frac{2}{\epsilon_1}} + \left(\frac{b^{-1}y}{T_y z + 1} \right)^{\frac{2}{\epsilon_1}} \right]^{\frac{\epsilon_1}{\epsilon_2}} + (c^{-1}z)^{\frac{2}{\epsilon_2}} \quad (8)$$

Ovoid

$$F_O(x, y, z) = \left(\frac{a^{-1}x}{c_{0x} + c_{1x}z + c_{2x}z^2 + c_{3x}z^3} \right)^2 + \left(\frac{b^{-1}y}{c_{0y} + c_{1y}z + c_{2y}z^2 + c_{3y}z^3} \right)^2 + (c^{-1}z)^2 \quad (9)$$

Superovoid

$$F_{SO}(x, y, z) = \left(\frac{a^{-1}x}{c_{0x} + c_{1x}z + c_{2x}z^2 + c_{3x}z^3} \right)^{\frac{2}{\epsilon_1}} + \left(\frac{b^{-1}y}{c_{0y} + c_{1y}z + c_{2y}z^2 + c_{3y}z^3} \right)^{\frac{2}{\epsilon_2}} + (c^{-1}z)^{\frac{2}{\epsilon_3}} \quad (10)$$

where $x, y, z \in R$ are the local coordinates of the point in space that belongs to the surface; $a, b, c \in R^+$ represent shape dimensions or semi-axis radii; $\epsilon_1, \epsilon_2, \epsilon_3 \in [0, 1]$ are the squareness parameters; $c_{0x}, c_{1x}, c_{2x}, c_{3x}, c_{0y}, c_{1y}, c_{2y}, c_{3y}$ are ovoidal shape coefficients, where the zero and first-degree coefficients $c_{0x}, c_{1x}, c_{0y}, c_{1y}$ are restricted to the range $[0, 1]$, while the second- and third-degree coefficients $c_{2x}, c_{3x}, c_{2y}, c_{3y}$ are limited to the interval $[-0.1, 0.1]$; T_x and T_y are the tapering values in the x and y directions, restricted between -1.0 and 1.0 .

The surfaces defined by (Equations 1–10) are represented in their respective local systems, where the referential origin

corresponds to the surfaces' centre. For modelling purposes, it is important to guarantee the possibility of granting the surface any spatial configuration. This geometrical modification consists in applying transformations to the surface's coordinate system, such as translation, rotation, and scaling.

Affine transformations are applied to the unit shape model, described by (Equations 1–10), by converting local coordinates, \mathbf{x} , to global coordinates, \mathbf{x}^* , by an affine matrix transformation that incorporates a scaling matrix, \mathbf{D} , that contains shape coefficients and dimension parameters (e.g. in millimetres) a, b , and c along the x, y , and z directions, a rotation matrix, \mathbf{R} , and a translation column vector, \mathbf{t} , which is expressed as a set of linear algebraic equations, which can be described in vector form by (Equation 11):

$$\mathbf{x}^* = [\mathbf{x}^* \mathbf{y}^* \mathbf{z}^* \mathbf{1}]^T = [\mathbf{R} \mathbf{D} \mathbf{t} \mathbf{0}_{1 \times 3} \mathbf{1}] \mathbf{x} \quad (11)$$

where \mathbf{x} and \mathbf{x}^* are written in homogeneous coordinates. Note that, the rotation matrix \mathbf{R} contains the information about the orientation of each local coordinate with respect to the global frame.

2.2 Image-based anatomical modelling

The articular surface geometry was extracted from CT data sets of a gender-balanced, asymptomatic population composed of 30 adult hip joints (14 male and 16 female subjects; 13 right-sided and 17 left-sided). All subjects are Caucasian and ages ranged from 18 to 44 years old (male: 32.7 ± 5.7 ; female: 28.6 ± 8.5). Young and relatively young healthy subjects were selected for this purpose, as older individuals have a higher risk of hip joint pathology. Data sets were gathered from two other studies (Harris et al. 2012; Lopes et al. 2018): (i), 20 CT scans of asymptomatic hip joints (512x512 acquisition matrix, in-plane and resolutions = 0.602–0.869 mm, slice thickness = 1.5–2 mm, 262–929 slices) acquired from the Hospital da Luz (Lisboa, Portugal) with a Siemens Emotion 16 (Siemens Healthineers, Germany) (Lopes et al. 2018); and (ii) 10 multi-detector CT scans of the pelvic region (512x512 acquisition matrix, in-plane x and y resolutions = 0.2155–0.2637 mm, slice thickness = 0.70–1.0 mm, and 241–357 slices) acquired from the University of Utah Hospital (Ahn 2004), which are available from the Musculoskeletal Research Laboratories at the University of Utah1 (Harris et al. 2012) All data sets were anonymised. All subjects had been informed of the intention to use their respective image sets and provided their written informed consent. The data sets used in our study resulted from the approval by the Ethics Research Committee of the Nova Medical School (nr.61/2014/CEFCM) (Lopes et al. 2018), and also by the University of Utah Institutional Review Board #10,983 (Harris et al. 2012).

The modelling pipeline begins with image segmentation of the bone–cartilage interface composing the femoral head and acetabular cavity¹. This process was performed with ITK-SNAP² (version 3.4) by using a combination of a semi-automatic method, that relied on 3-D active contour evolution (Yushkevich et al. 2006), and manual segmentation to correct errors. The segmented images were then imported into ParaView³ (version 4.3.1), in order to create a triangle mesh with the marching cubes algorithm (Lorensen and Cline 1987).

Mesh decimation and Laplacian filtering were then applied to remove the excessive vertex number and smooth mesh artefacts, such as voxelised features. Furthermore, the regions corresponding to the articular surfaces of the hip joint were manually selected from the surface model in Blender⁴ (version 2.75), so that the underlying point cloud resulting from the remaining vertices of the surface model could be stored.

2.3 Surface-fitting analysis

Implicit surface fitting of the 10 geometric primitives is performed taking the extracted point clouds as input. Goodness-of-fit or surface error is analysed and compared based on the Euclidean distance between the input points and the optimally fitted surfaces. To obtain these errors, an orthogonal distance optimisation framework is taken into account, which needs to satisfy a non-linear equality constraint given by the implicit surface equation. Both surface-fitting and the surface error calculations are accomplished in Matlab[®] (version R2014a) using the Genetic Algorithm and Direct Search Toolbox[™] and the code ran on an Intel[®] Core™ i5 processor 2.4 GHz and 5 GB of RAM. To better understand the goodness of fit of each of the geometric primitives, a qualitative and quantitative analysis is performed on the fitting results using the surface errors.

For a point cloud with $n \in N$ points in Cartesian space belonging to the outer cortical bone surface of the hip joint, the vector of geometric parameters $\lambda \in R^m$, where $m \in N$ is the number of parameters characterising a given implicit surface, which minimises the EOF objective function, $EOF(\lambda)$, was determined. This objective function is defined as the square sum of residual function f for each point $i = \{1, \dots, n\}$, where f is the difference between the shape model function and the i th point datum, as formulated by the following expression

$$EOF(\lambda) = \sum_{i=1}^n f_i^2(x_g, y_g, z_g; \lambda) = \sum_{i=1}^n (1 - F_i(x_g, y_g, z_g; \lambda))^2 \quad (12)$$

under the restriction

$$l \leq \lambda \leq u \quad (13)$$

where F is the implicit surface representation of a given shape model and $l, u \in R^m$ are the lower and upper bound column vectors, respectively, setting the limits for the solution presented in λ . In addition to the parameters needed to define each shape model, such as curvature and, in the case of ovoids,

conicity, the vector λ also includes the rotation and translation factors used in the affine transformations. It is, therefore, a vector of global anatomical information. As for the EOF objective function domain,

(Table 2) summarises the different shape models used in the studies and the vector of geometric parameters associated with each of them. For the shape models that include squareness parameters, and since $\epsilon_1, \epsilon_2, \epsilon_3$ are confined to be greater than 0 and lesser than 1, the gamma exponents are represented as $\gamma = \frac{2}{\epsilon}$. Note that for surfaces exhibiting exponents larger than 2, the change in exponent representation means that γ_1, γ_2 and γ_3 are restricted to the range $[2, +\infty]$.

The surface-fitting error is expressed as the minimum distance between each point of the point cloud and the optimally fitted surface, also called signed Euclidean distance, SED , was computed as:

$$SED(x_{OS}; x_{OP}) = \min_{x_{OS}} \text{sign}(F(x_{OP})) \|x_{OP} - x_{OS}\|_2 = \min_{x_{OS}} \|d_{PS}\|_2 \quad (14)$$

and must respect the non-linear equality constraint

$$F(x_{OS}; \lambda^*) = 1 \quad (15)$$

where $x_{OS} \in R^3$ is a point belonging to the fitted surface and x_{OP} is a point from the point cloud which can lie inside, outside or on top of the surface; $\text{sign}(\cdot)$ is the sign function; $d_{PS} \in R^3$ represents the distance vector between point P of the point cloud and the iterated surface point S, F is the implicit surface representation for each of the geometric primitives given by (Equations 1–10); and λ^* is the vector of geometric parameters characterising the optimally fitted surface. Note that (Equation 14) expresses the physical distance between each point of the reconstructed hip surface to the optimally fitted shape, hence, can be used to measure the surface-fitting error.

2.4 Shape metrics

Several metrics that quantify deviations from the sphere shape were used to characterise hip joints. Given the close resemblance between synovial ball-and-socket joint morphology and egg-like shapes (MacConaill 1966, 1973; Standing 2015), we adopted metrics found in ornithology (Carter 1968; Paganelli et al. 1974; Afoke et al. 1980; Todd and Smart 1984). Interestingly, zoologists and ornithologists consider that there are three types of avian egg shapes: spherical, elliptical and conical (Stoddard et al. 2017).

Table 2. Vector of geometric parameters for all shape models considered and the respective number of degrees of freedom, given by the total number of surface parameters, m .

Shape model	λ	m
S	$\lambda_s = [a, t_1, t_2, t_3]^T$	4
RC	$\lambda_{RO} = [a, b, t_1, t_2, t_3, \phi, \theta, \psi]^T$	8
RE	$\lambda_{RE} = [a, b, t_1, t_2, t_3, \phi, \theta, \psi]^T$	8
E	$\lambda_E = [a, b, c, t_1, t_2, t_3, \phi, \theta, \psi]^T$	9
SE	$\lambda_{SE} = [a, b, c, \gamma_1, \gamma_2, \gamma_3, t_1, t_2, t_3, \phi, \theta, \psi]^T$	12
SEB	$\lambda_{SEB} = [a, b, c, \gamma_1, \gamma_2, t_1, t_2, t_3, \phi, \theta, \psi]^T$	11
TE	$\lambda_{TE} = [a, b, c, T_x, T_y, t_1, t_2, t_3, \phi, \theta, \psi]^T$	11
TSEB	$\lambda_{TSEB} = [a, b, c, \gamma_1, \gamma_2, T_x, T_y, t_1, t_2, t_3, \phi, \theta, \psi]^T$	13
O	$\lambda_O = [a, b, c, c_{0x}, c_{1x}, c_{2x}, c_{3x}, c_{0y}, c_{1y}, c_{2y}, c_{3y}, t_1, t_2, t_3, \phi, \theta, \psi]^T$	17
SO	$\lambda_{SO} = [a, b, c, \gamma_1, \gamma_2, \gamma_3, c_{0x}, c_{1x}, c_{2x}, c_{3x}, c_{0y}, c_{1y}, c_{2y}, c_{3y}, t_1, t_2, t_3, \phi, \theta, \psi]^T$	20

Correspondingly, each avian shape presents a main feature: sphericity, ellipticity (or flattening), and conicity (or asymmetry).

Sphericity quantifies how closely the shape of an object approaches that of a sphere. It can be measured by comparing the difference between the surface-fitting errors of each shape to those of the sphere (Equation 14). As for ellipticity, it refers to how much a shape deviates from being spherical as if it resulted from compressing a sphere along a given diameter to form an ellipsoid of revolution. Regarding conicity, it measures how pointy a shape is, i.e. how much a shape is axial asymmetric. Although ellipticity and conicity are standard metrics to quantify egg-like shapes, other parameters can be introduced to attempt better descriptions of hip joint morphology. Following previous work on femoral head morphology (Lopes et al. 2015), we also considered squareness that measures how close a shape is to a box form. In short, the performed shape analysis took into account four shape metrics: sphericity, ellipticity, conicity and squareness. Table 3 lists the formulas for each shape and associated metric.

Note that shape metrics are expressed, by definition, as a ratio between parameters of two-dimensional curves (e.g. eccentricity of an ellipse). Since we are dealing with three-dimensional objects, each formula in (Table 3) accounts for shape measurements in the xOy, xOz, and yOz planes expressed in local coordinates.

2.5 Statistical analyses

The quantitative analyses of the limit of hip sphericity relied on the surface-fitting errors that are quantified by the signed Euclidean distances, i.e. distance of each point in a point cloud to the optimally fitted surface of each shape model (points laying on the surface have zero valued distance, points inside the surface have 'negative distances', while points outside have positive valued distance). Surface-fitting errors were estimated across the 30 pelvic bones and compared between the 10 shapes. To compare the surface-fitting results of the different shape models, we conducted two statistical analyses (Marusteri and Bacarea 2010; Ghasemi and Saleh 2012). First, we measured descriptive statistics to describe the main features of data in quantitative terms, e.g. first-order statistics such as mean, standard deviation, minimum, maximum, and root

mean square (RMS) error values. Second, we aimed to verify if different shapes have an effect on shape morphology through statistical hypothesis testing to verify which shape fits best. Gender variability was also quantified by comparing ellipticity, conicity and squareness among several different shapes.

Regarding statistical hypothesis testing, we took surface-fitting error as a continuous measurement variable and shape as a nominal variable whilst we assume, as a null hypothesis, that different shapes do not affect the surface-fitting error, equivalently, as an alternate hypothesis that different shapes have different averages of surface-fitting error. To verify if the surface-fitting errors represent observable differences between the means of the surface-fitting errors, it was necessary to check for normality to decide which type of statistical test is more appropriate for statistical reasoning. Normality tests indicate that the sample data does not follow a well-modelled normal distribution. All surface-fitting error datasets were evaluated for normality using the Shapiro–Wilk test that provides sufficient statistical confidence that the population is far from normally distributed. By computing population kurtosis, k , we verified that data was substantially skewed data or flat ($k > 0.5$). Since the surface-fitting error does not follow a normal distribution, we applied the Kruskal–Wallis test (Ghasemi and Saleh 2012). Pairwise comparisons among the shape groups were accomplished by selecting two groups at a time and by running a separate Kruskal–Wallis test for each pair. A statistically significant result was given a p -value < 0.05 .

3. Results

The initial assessment of the overall goodness-of-fit of the approximated surfaces, performed by visual examination, suggests that the chosen shape models adjust well to the global anatomy of the articular surfaces for all data sets of the femoral head (Figure 3) and acetabular cavity (Figure 4). Along with visual inspection, the statistical metrics provided insight on whether the surface parameters have anatomical meaning and how well-adjusted shapes performed in terms of dispersion and central tendency. In order to improve the general understanding of the discussion, statistical results for femoral and acetabular cases are presented separately. The full list of the estimated femoral head and acetabular cavity shape parameters is presented in (Supporting Information: Table 1) and (Supporting Information: Table 2), respectively.

Table 3. Shape metric formulas of the non-spherical shapes. All metrics are strictly lesser than 1. Near zero values for ellipticity and conicity correspond to shapes similar to the perfect sphere, while squareness values closer to 2.0 are more similar to a sphere. Higher values of ellipticity result in oblate or prolate spheroid shapes. Increasing values of conicity accentuate the egg-like protrusion. Growing values of squareness result in a more squared shape. With exception to the rotational conchoid, shape dimensions satisfy the inequality expression of $a \geq b \geq c$.

	Ellipticity	Conicity	Squareness
Rotational conchoid	-	$2\frac{a}{b}$	-
Rotational ellipsoid	$1 - \frac{b}{a}$	-	-
Ellipsoid	$\frac{(1 - \frac{b}{a} + 1 - \frac{c}{a} + 1 - \frac{c}{b})}{3}$	-	-
Superellipsoid	$\frac{(1 - \frac{b}{a} + 1 - \frac{c}{a} + 1 - \frac{c}{b})}{3}$	-	$\frac{\frac{2}{\epsilon_1} + \frac{2}{\epsilon_2} + \frac{2}{\epsilon_3}}{3}$
Barr's superellipsoid	$\frac{(1 - \frac{b}{a} + 1 - \frac{c}{a} + 1 - \frac{c}{b})}{3}$	-	$\frac{\frac{2}{\epsilon_1} + \frac{2}{\epsilon_2}}{2}$
Tapered ellipsoid	$\frac{(1 - \frac{b}{a} + 1 - \frac{c}{a} + 1 - \frac{c}{b})}{3}$	$\frac{ T_x + T_y }{2}$	-
Barr's tapered superellipsoid	$\frac{(1 - \frac{b}{a} + 1 - \frac{c}{a} + 1 - \frac{c}{b})}{3}$	$\frac{ T_x + T_y }{2}$	$\frac{\frac{2}{\epsilon_1} + \frac{2}{\epsilon_2}}{2}$
Ovoid	$\frac{(1 - \frac{b}{a} + 1 - \frac{c}{a} + 1 - \frac{c}{b})}{3}$	$\frac{\sum_{i,j}^{x,y} c_{0i} + c_{1j} + c_{2i} + c_{3j} }{4.4}$	-
Superovoid	$\frac{(1 - \frac{b}{a} + 1 - \frac{c}{a} + 1 - \frac{c}{b})}{3}$	$\frac{\sum_{i,j}^{x,y} c_{0i} + c_{1j} + c_{2i} + c_{3j} }{4.4}$	$\frac{\frac{2}{\epsilon_1} + \frac{2}{\epsilon_2} + \frac{2}{\epsilon_3}}{3}$

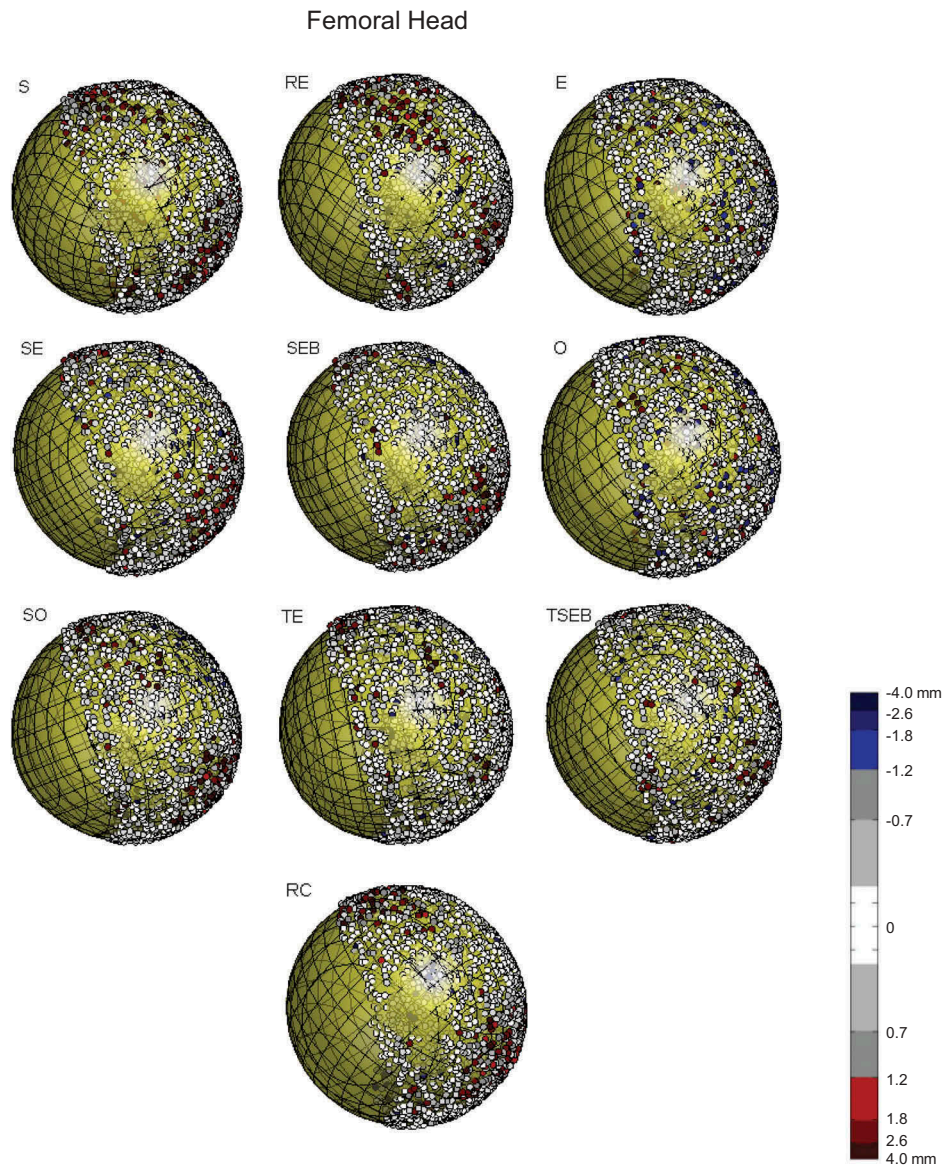


Figure 3. A 3-D view of the optimally fitted surfaces for the femoral head of subject 11. Point clouds are coloured according to the Euclidean distance between the point and approximated surface. Surface error colour map: inner points are represented in blue; outer points are coloured in red; points close to the surface are represented in a greyscale.

The point clouds in (Figures 3 and 4) are coloured as a function of each point's Euclidean distance to the optimally fitted surface. The colour code uses three gradients: points located inside the surface below -1.0 mm are given the colour red whose intensity increases with the distance to the surface; exterior points located above 1.0 mm of the surface are given the colour blue following the same intensity criterion as the interior points; and all points within -1.0 mm and 1.0 mm of distance to the approximated surface are coloured in a greyscale, where brighter shades correspond to smaller distances with white being the zero distance.

3.1 Limit of sphericity of the femoral head

(Table 4) promptly represents how the fitting errors distribute among the different shapes and it is possible to observe the overall similarity and variability in range values, mean and

standard deviation between all shape models. To better illustrate the distribution of fitting errors between genders and ages, a heat map representing the individual values of RMS for each subject and shape is presented in (Figure 5). Sorted by age, the heat map is divided into top and bottom sections to list male and female subjects, respectively.

From (Table 4) and (Figure 5) it is possible to easily discern that spheres provided the worst fit, whereas egg-like shapes present the lowest fitting errors. Interestingly, there was no statistical significance between sphere and all the remaining shapes ($p \geq 0.05$); hence, the overall medians of each shape group are not different for both male and female subjects (Table 5). In its turn, rotational conchoids, rotational ellipsoids and ellipsoids are statistically different from superellipsoidal and egg-like shapes, although the differences were not significant between superellipsoidal shapes (SE, SEB) or between egg-like shapes (TE, TSEB, O, SO).

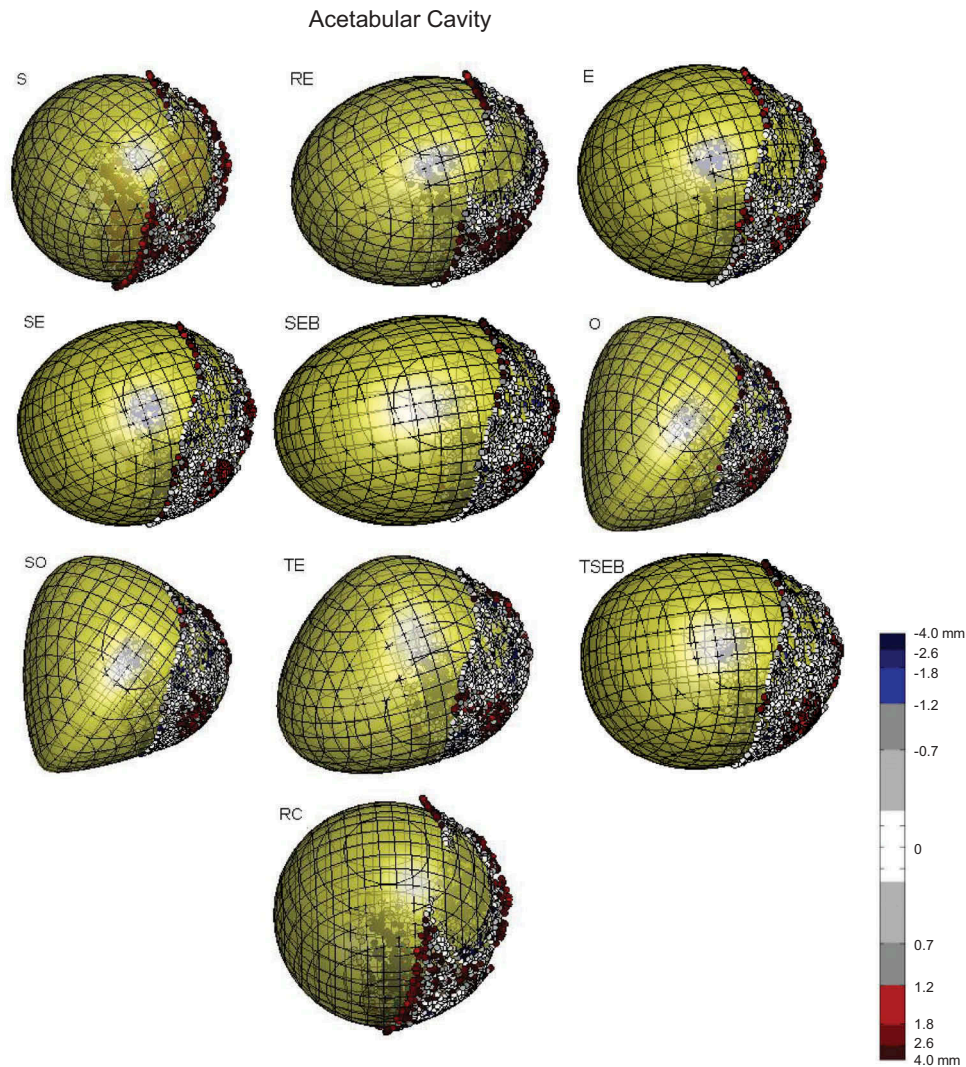


Figure 4. A 3-D view of the optimally fitted surfaces for the acetabular cavity of subject 11. Point clouds are coloured according to the Euclidean distance between the point and approximated surface. Surface error colour map: inner points are represented in blue; outer points are coloured in red; points close to the surface are represented in a grey scale.

3.2 Limit of sphericity of the acetabular cavity

Similar to the femoral case, a quantitative analysis of the differences between shapes and respective goodness-of-fit to acetabular point clouds was performed. Table 6 lists first-order statistics of the surface-fitting errors and the RMS of total fitting errors for each shape model which contribute to the understanding of how error values are distributed along each shape. A heatmap of the RMS for each subject and shape was also generated to visually represent the distribution of fitting errors between genders and ages (Figure 6).

A closer look at the results of Table 6 and Figure 6 bespeaks the same tendency previously found in the femoral cases for both male and female groups. Goodness-of-fit improves progressively for shape primitives which present increasing asphericity, culminating in egg-like shapes with the best fitting values. By comparing the differences between the surface-fitting errors (Tables 4 and 6), an expected result emerges as the acetabular cavity is indeed better established as a non-spherical articular surface than the femoral head. A paired Kruskal–Wallis was also used to classify the significance of the

differences between fitting errors of all shape models. Statistical significance was once again set at $p < 0.05$. The pairs which demonstrated significant results are highlighted in Table 7. Curiously, the acetabular cavity presents a slightly greater amount of shape pairs where the differences between fitting errors are significantly different. Even so, the difference between fitting errors was still significantly different between either TE or SO and ellipsoidal shapes (RC, RE, E) and super-ellipsoidal shapes (SE, SEB).

3.3 Other shape metrics

By evaluating the different shape metric formulas described in (Table 3), it is possible to address how hip joint ellipticity, conicity and squareness vary among both genders when comparing each gender metric for a given shape (Tables 8 and 9). These tabulated results indicate that male and female hips have very similar shape metrics. Only minute differences indicate that the female femoral head is slightly more asymmetric and squared than male hips. The same occurs for the acetabular

Table 4. Surface-fitting errors statistical analysis of the femoral head for each shape model, for each gender and the whole population present in the study (30 subjects). All metrics are represented in millimetres (mm). The mean and standard deviation are calculated for the absolute value of the surface error. Min and Max values are represented based on the minimal signed Euclidean distances calculated between each point and the optimal fitted shape.

Gender comparison		Femoral Head									
		S		RC		RE		E		SE	
		M	F	M	F	M	F	M	F	M	F
μ	0.650	0.651	0.619	0.519	0.623	0.600	0.594	0.563	0.567	0.499	
σ	0.573	0.556	0.558	0.471	0.549	0.542	0.534	0.521	0.525	0.468	
Min	-4.051	-4.091	-2.775	-2.843	-2.879	-2.784	-2.857	-2.683	-2.704	-2.789	
Max	0.072	2.376	3.747	3.569	3.973	4.099	3.779	3.862	3.639	3.509	
RMS	0.867	0.863	0.833	0.701	0.830	0.809	0.799	0.767	0.773	0.685	
Study population		SEB		TE		TSEB		O		SO	
		M	F	M	F	M	F	M	F	M	F
		μ	0.577	0.516	0.539	0.520	0.550	0.467	0.526	0.460	0.526
σ	0.522	0.482	0.519	0.495	0.517	0.444	0.508	0.443	0.499	0.437	
Min	-2.761	-2.671	-2.961	-2.901	-2.586	-2.640	-2.747	-2.823	-2.586	-2.737	
Max	3.730	3.476	3.752	3.658	3.627	3.633	3.867	3.405	3.673	3.407	
RMS	0.778	0.706	0.749	0.718	0.755	0.645	0.731	0.639	0.725	0.632	
Study population		S	RC	RE	E	SE	SEB	TE	TSEB	O	SO
μ	0.651	0.565	0.610	0.577	0.531	0.544	0.529	0.506	0.490	0.489	
σ	0.570	0.516	0.545	0.527	0.496	0.502	0.507	0.481	0.475	0.468	
Min	-4.496	-2.843	-2.795	-2.857	-2.789	-2.761	-2.961	-2.640	-2.823	-2.737	
Max	2.376	3.747	4.099	3.862	3.639	3.730	3.752	3.633	3.866	3.673	
RMS	0.865	0.765	0.819	0.782	0.727	0.740	0.733	0.698	0.683	0.677	

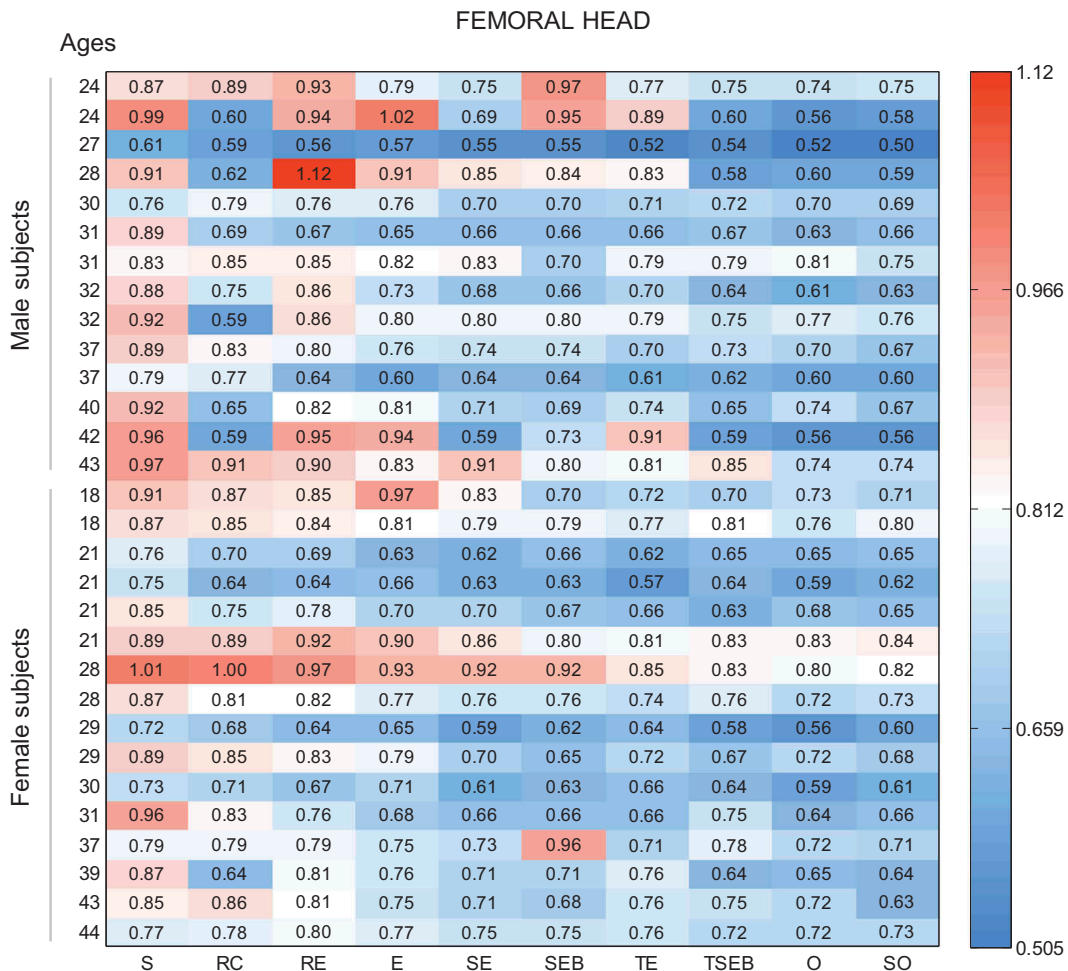


Figure 5. Heat map of the surface-fitting errors of the femoral heads for the study population. A single row contains the RMS fitting errors for a subject (in mm), while each column corresponds to a different shape.

Table 5. Statistical significance of the differences between fitting errors for all shape models for the femoral head, using paired Kruskal–Wallis tests with statistical significance set at $p < 0.05$. The lower triangular half and upper triangular half correspond to the male and female groups, respectively.

		Femoral head								
	S	RC	RE	E	SE	SEB	TE	TSEB	O	SO
S	-	1.000	1.000	1.000	1.000	1.000	1.000	1.000	1.000	1.000
RC	1.000	-	0.000	0.311	0.067	0.475	0.001	0.007	0.001	0.040
RE	1.000	0.110	-	0.014	0.000	0.000	0.000	0.000	0.000	0.000
E	1.000	0.001	0.130	-	0.005	0.099	0.000	0.000	0.000	0.003
SE	1.000	0.000	0.016	0.408	-	0.278	0.141	0.415	0.124	0.915
SEB	1.000	0.000	0.000	0.014	0.077	-	0.012	0.062	0.009	0.238
TE	1.000	0.000	0.000	0.009	0.051	0.916	-	0.433	0.939	0.139
TSEB	1.000	0.000	0.000	0.034	0.149	0.599	0.664	-	0.481	0.450
O	1.000	0.000	0.000	0.006	0.034	0.979	0.859	0.550	-	0.142
SO	1.000	0.000	0.000	0.070	0.253	0.368	0.401	0.681	0.309	-

Bold values refer to p-values lesser than 0.05.

Table 6. Surface-fitting errors statistical analysis of the acetabular cavity for each shape model, for each gender and the whole population present in the study (30 subjects). All metrics are represented in millimetres (mm). The mean and standard deviation are calculated for the absolute value of the surface error. Min and Max values are represented based on the minimal signed Euclidean distances calculated between each point and the optimal fitted shape.

		Acetabular cavity									
		S		RC		RE		E		SE	
Gender comparison		M	F	M	F	M	F	M	F	M	F
	μ	1.022	0.982	0.995	0.968	0.874	0.832	0.849	0.808	0.836	0.800
	σ	0.766	0.651	0.749	0.645	0.704	0.592	0.689	0.579	0.663	0.590
	Min	-3.996	-3.857	-3.748	-3.585	-3.985	-4.092	-3.786	-3.857	-3.649	-3.508
	Max	0.000	1.476	3.464	3.054	3.986	2.872	3.787	3.169	3.590	3.078
	RMS	1.277	1.178	1.246	1.163	1.121	1.021	1.094	0.994	1.098	0.994
		SEB		TE		TSEB		O		SO	
		M	F	M	F	M	F	M	F	M	F
	μ	0.754	0.774	0.767	0.719	0.766	0.702	0.758	0.718	0.742	0.682
	σ	0.649	0.568	0.602	0.538	0.614	0.538	0.621	0.540	0.600	0.534
	Min	-3.747	-3.472	-3.746	-3.553	-3.692	-3.134	-3.878	-3.004	-3.660	-3.093
	Max	3.624	2.934	3.218	3.102	3.047	2.684	3.862	2.749	3.231	2.768
	RMS	1.058	0.960	0.965	0.898	0.983	0.885	0.980	0.898	0.954	0.866
Study population		S	RC	RE	E	SE	SEB	TE	TSEB	O	SO
	μ	1.000	0.980	0.851	0.827	0.835	0.803	0.735	0.732	0.737	0.709
	σ	0.707	0.696	0.646	0.634	0.626	0.607	0.569	0.576	0.579	0.566
	Min	-4.497	-3.748	-4.092	-3.857	-3.649	-3.747	-3.746	-3.692	-3.878	-3.660
	Max	1.476	3.464	3.464	3.464	3.463	3.463	3.218	3.047	3.464	3.231
	RMS	1.225	1.202	1.069	1.042	1.043	1.007	0.929	0.932	0.937	0.908

cavity, with the addition of female hips being slightly more flattened although notoriously more asymmetric than male acetabular cavities.

In addition, shape parameters (Supporting Information: Table 1; Supporting Information: Table 2) reveal that the calculated ovoidal coefficients are within the boundaries established by Todd and Smart (Todd and Smart 1984) to describe avian eggs. Moreover, the calculated exponent values of superellipsoids, Barr's superellipsoids, Barr's tapered superellipsoids and superovoids are extremely close to the quadratic values, despite the maximum of $\gamma = 2.25$. As for the rotational conchoids, all optimally shapes have a ratio between the largest and smallest shape parameters lesser or equal to 2; hence, each computed shape is a convex limaçon.

4. Discussion

The human femoral head and acetabular shape are commonly represented as a sphere or hemisphere, but there have been no extensive quantitative assessments of this assumption in the literature. The work by MacConaill introduced the idea that the

hip joint, along with other spheroidal joints, did not present geometrical features most consistent with a sphere, but with ovoidal shapes, instead (MacConaill 1966; Williams et al. 2010). In this work, we evaluated shape variation and tested the limit of the hip joint sphericity assumption by comparing the largest set of shapes adjusted to 3D reconstructions of femoral heads and acetabular cavities. Our aim was to contribute to the ongoing debate and to test the limits and validity of this hypothesis by comparing 10 different parameterisations. The considered shape primitives present a compact number of geometric modelling parameters which are intuitive, easily controllable, are able to describe macroscopic features of the femoral head and acetabular cavity, namely, ellipticity, conicity and squareness. We also addressed how such shape features vary among both sexes.

In conclusion, we can synthesise that the osseous morphology of the femoral head and acetabular cavity, of both genders, can be parameterised by superovoids with superior quality than the simple sphere shape. There exists a clear distinction between spheres and egg-like shapes: spheres have the worst fitting metrics, while superovoids have the lowest surface-

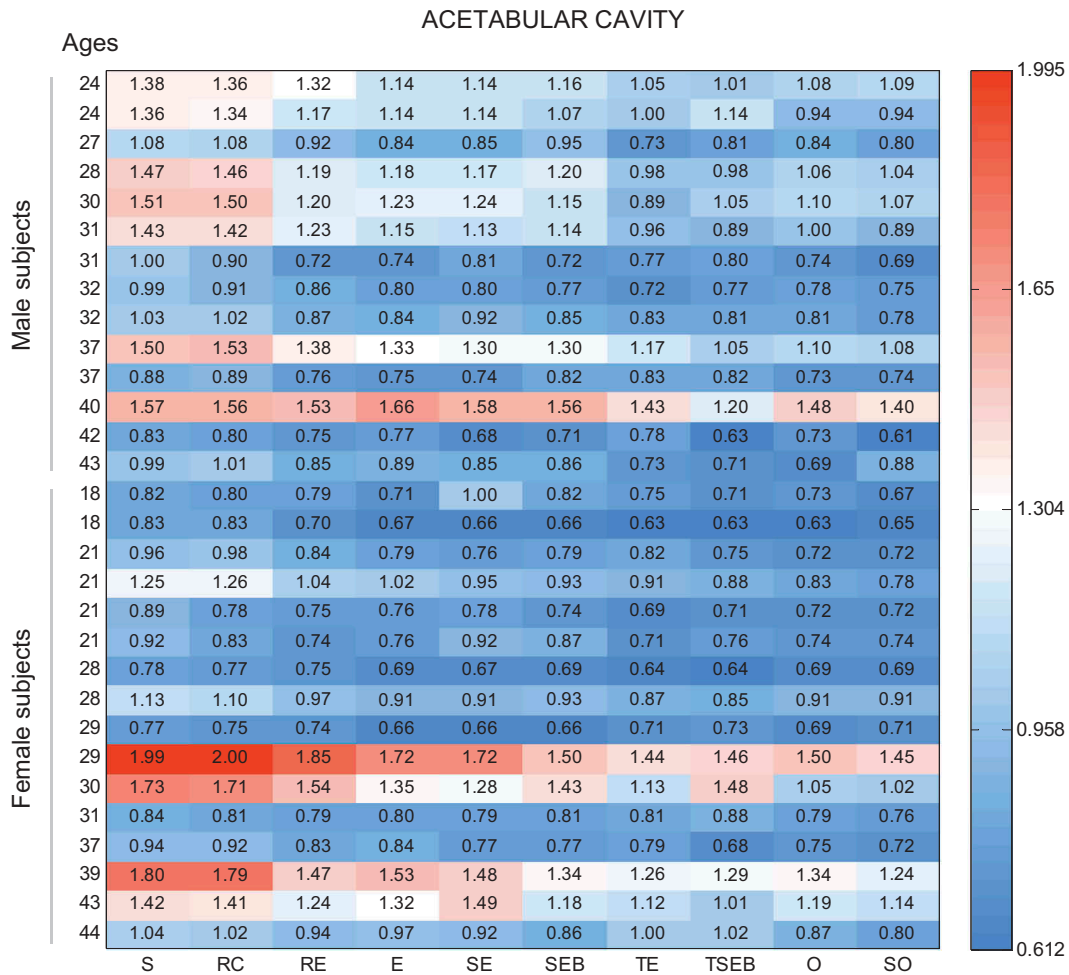


Figure 6. Heat map of the surface-fitting errors of the acetabular cavities for the study population. A single row contains the RMS fitting errors for a subject (in mm), while each column corresponds to a shape.

Table 7. Statistical significance of the differences between fitting errors for all shape models for the acetabular cavity, using paired Kruskal–Wallis tests with statistical significance set at $p < 0.05$. The lower triangular half and upper triangular half correspond to the male and female groups, respectively.

	Acetabular cavity									
	S	RC	RE	E	SE	SEB	TE	TSEB	O	SO
S	-	1.000	1.000	1.000	1.000	1.000	1.000	1.000	1.000	1.000
RC	1.000	-	0.000	0.000	0.000	0.000	0.000	0.000	0.000	0.000
RE	1.000	0.000	-	0.939	0.178	0.239	0.000	0.001	0.000	0.000
E	1.000	0.000	0.035	-	0.157	0.190	0.000	0.000	0.000	0.000
SE	1.000	0.000	0.593	0.114	-	0.900	0.007	0.022	0.000	0.000
SEB	1.000	0.000	0.054	0.844	0.159	-	0.005	0.016	0.000	0.000
TE	1.000	0.000	0.000	0.037	0.000	0.019	-	0.592	0.180	0.182
TSEB	1.000	0.000	0.122	0.518	0.314	0.668	0.004	-	0.063	0.055
O	1.000	0.000	0.000	0.138	0.002	0.082	0.528	0.027	-	0.999
SO	1.000	0.000	0.000	0.029	0.000	0.015	0.886	0.003	0.432	-

Bold values refer to p-values lesser than 0.05.

fitting errors throughout the entire study population. As for shapes previously considered in hip morphology literature (e.g. rotational conchoids, rotational ellipsoids and ellipsoids), they lie within the spherical and oval extremities of the surface-fitting error spectrum, as such shapes are more limited in terms of representing morphological inter- and intra-subject-specific variations. In its turn, ovoidal shapes present a greater level of generalisation, brought to some extent by the conicity parameters which account for greater shape complexity and

individual morphology variation. Therefore, ovoidal shapes exhibited better fitting results for the study population.

From the comparison between the femoral head surface-fitting errors listed in (Tables 4 and 6), it is possible to conclude that the goodness-of-fit of the distinct shape models follows the same pattern for individual subjects as for the population as a whole. Relative to the femoral head, Table 4 allows the establishment of the asphericity relationships between the different shape models, ordered according to decreasing RMS surface-fitting error:

Table 8. Shape metrics measured for the femoral head of male and female subjects. All metrics are normalised with the exception of squareness.

		Ellipticity		Conicity		Squareness	
		M	F	M	F	M	F
RC	μ	-	-	0.229	0.247	-	-
	σ	-	-	0.179	0.179	-	-
	Min	-	-	0.002	0.002	-	-
	Max	-	-	0.520	0.520	-	-
RE	μ	0.040	0.043	-	-	-	-
	σ	0.021	0.023	-	-	-	-
	Min	0.013	0.013	-	-	-	-
	Max	0.074	0.087	-	-	-	-
E	μ	0.045	0.045	-	-	-	-
	σ	0.018	0.017	-	-	-	-
	Min	0.017	0.017	-	-	-	-
	Max	0.073	0.073	-	-	-	-
SE	μ	0.045	0.044	-	-	2.070	2.079
	σ	0.027	0.026	-	-	0.047	0.053
	Min	0.013	0.013	-	-	2.003	2.003
	Max	0.113	0.113	-	-	2.193	2.193
SEB	μ	0.074	0.071	-	-	2.118	2.124
	σ	0.073	0.069	-	-	0.069	0.072
	Min	0.014	0.014	-	-	2.012	2.012
	Max	0.260	0.260	-	-	2.250	2.250
TE	μ	0.052	0.050	0.132	0.132	-	-
	σ	0.048	0.046	0.128	0.124	-	-
	Min	0.011	0.011	0.020	0.020	-	-
	Max	0.179	0.179	0.454	0.454	-	-
TSEB	μ	0.107	0.097	0.174	0.159	2.055	2.063
	σ	0.091	0.089	0.154	0.149	0.051	0.056
	Min	0.005	0.005	0.029	0.029	2.009	2.009
	Max	0.265	0.265	0.466	0.466	2.168	2.169
O	μ	0.041	0.043	0.506	0.509	-	-
	σ	0.019	0.023	0.019	0.020	-	-
	Min	0.014	0.014	0.484	0.484	-	-
	Max	0.072	0.092	0.535	0.537	-	-
SO	μ	0.036	0.040	0.509	0.509	2.056	2.058
	σ	0.017	0.020	0.025	0.024	0.054	0.052
	Min	0.009	0.009	0.468	0.468	2.003	2.003
	Max	0.062	0.085	0.539	0.539	2.165	2.165

Table 9. Shape metrics measured for the acetabular cavity of male and female subjects. All metrics are normalised with the exception of squareness.

		Ellipticity		Conicity		Squareness	
		M	F	M	F	M	F
RC	μ	-	-	0.229	0.255	-	-
	σ	-	-	0.252	0.246	-	-
	Min	-	-	0.002	0.002	-	-
	Max	-	-	0.735	0.735	-	-
RE	μ	0.109	0.125	-	-	-	-
	σ	0.194	0.186	-	-	-	-
	Min	-0.345	-0.345	-	-	-	-
	Max	0.316	0.316	-	-	-	-
E	μ	0.118	0.113	-	-	-	-
	σ	0.029	0.036	-	-	-	-
	Min	0.083	0.024	-	-	-	-
	Max	0.198	0.198	-	-	-	-
SE	μ	0.154	0.153	-	-	2.064	2.061
	σ	0.053	0.050	-	-	0.062	0.060
	Min	0.093	0.093	-	-	2.000	2.000
	Max	0.275	0.275	-	-	2.179	2.178
SEB	μ	0.134	0.135	-	-	2.161	2.177
	σ	0.061	0.057	-	-	0.194	0.201
	Min	0.042	0.042	-	-	2.000	2.000
	Max	0.303	0.303	-	-	2.501	2.500
TE	μ	0.122	0.124	0.207	0.216	-	-
	σ	0.055	0.055	0.124	0.121	-	-
	Min	0.033	0.033	0.063	0.063	-	-
	Max	0.261	0.261	0.496	0.496	-	-
TSEB	μ	0.114	0.122	0.134	0.151	2.133	2.137
	σ	0.055	0.063	0.077	0.093	0.170	0.161
	Min	0.046	0.046	0.023	0.023	2.001	2.001
	Max	0.236	0.260	0.258	0.376	2.500	2.500
O	μ	0.117	0.118	0.557	0.564	-	-
	σ	0.028	0.027	0.035	0.038	-	-
	Min	0.080	0.080	0.508	0.508	-	-
	Max	0.186	0.186	0.615	0.618	-	-
SO	μ	0.114	0.115	0.542	0.549	2.034	2.035
	σ	0.029	0.027	0.037	0.039	0.055	0.053
	Min	0.077	0.077	0.479	0.479	2.000	2.000
	Max	0.181	0.181	0.600	0.611	2.177	2.170

Male $S > RC > RE > E > SEB > SE > TSEB > TE > O > SO$
 Female $S > RE > E > TE > SEB > RC > SE > TSEB > O > SO$
 Study population $S > RE > E > RC > SEB > TE > SE > TSEB > O > SO$ (16)

The inequality condition (Equation 16) expresses a clear division between two sets of surfaces, namely, spheres and ovoids. In addition Equation (16) reveals that ellipticity alone does not lead to cost-efficient analyses, given that RE, E, SE and SEB shapes presented worse fitting results than ovoids and superovoids. Although the differences in the statistical measures presented are not of a high magnitude, the geometric features of the two shapes with highest and lowest fitting errors are undoubtedly distinct, despite the morphometric changes which transform one into the other.

Regarding the acetabular cavity, Table 6 reveals the comparison between the RMS of the surface-fitting errors for the 10 different shapes, which results in the following inequality relation established after decreasing RMS surface-fitting error:

Male $S > RC > RE > SE > E > SEB > TSEB > O > TE > SO$
 Female $S > RC > RE > E > SE > SEB > TE > O > TSEB > SO$
 Study population $S > RC > RE > SE > E > SEB > O > TSEB > TE > SO$ (17)

When cross-checked with the comparison drawn for the femoral case, a shape polarisation becomes very evident (Equation 16 and equation 17): spheres on one end and ovoids on the other end of the surface-fitting spectrum, with the remaining shapes occupying in-between positions. It is also worthwhile to highlight that the RMS values of the surface-fitting errors of the femoral head were lower than the ones observed for the acetabular cavity, which emphasises the notion that the femoral head is a more spherical structure than the acetabulum.

In short, the results from surface-fitting analyses demonstrate that the sphere is not the most representative hip joint shape. In fact, the best fit is an egg shape which contains a well-balanced combination of ellipticity, conicity and squareness. The performed shape metric analyses also reveal how hip anatomy differs between males and females regarding sphericity, ellipticity, conicity and squareness vary among sexes. An overall comparison of the shape metrics performed on the study population revealed just minute gender differences (Tables 8 and 9). On average, the female femoral head is more asymmetric and squared comparatively to the male counterpart, which in turn is slightly more flat. Whereas, the female acetabular cavity is more flat, asymmetric and squared when compared to male hips. Therefore, the distribution of observed shape metrics indicates morphological similarity between genders.

The results indicate that the femoral head and acetabular cavity, in asymptomatic conditions, approximate better to ovoidal geometries, in detriment to spherical ones, hence, corroborates the idea introduced by MacConaill (1966, 1973) and reinforces the need to change the global understanding of the hip joint established within the radiologic orthopaedic community, considering that the computer-aided tools used currently for orthopaedic pre-surgical planning rely on spherical geometries for the articular surfaces of the hip joint (Lopes et al. 2018).

Moreover, the shape primitives with the lowest RMS of surface-fitting errors for the femoral head and the acetabular cavity are not especially distant from each in both orders of goodness-of-fit. This lack of shape model match between the articular surfaces is frequently described in the orthopaedic community as 'incongruity' and it implies a difference in the contact area between the two surfaces dependent on the applied stress/load on the joint. Lighter or lower loads lead to limited contact, while heavier or higher loads conduce to an increase in the contact area. The existence of this incongruity generates space between the two articular surfaces, which is thought to be a way of distributing load and protecting the cartilage from undue stress while giving synovial fluid access for lubrication and nutrition of the joint. Also, incongruity is commonly determined by an arched acetabulum and a rounded femoral head (Afoke et al. 1980; Cooper et al. 2017).

An important aspect that rarely appears in the literature, but deserves to be mentioned are the issues related to systematic error due to 3D reconstruction. Although implicit surface representations allow for infinite resolution and accuracy-controlled point-surface distance computations (Equations 1–10), the surface-fitting errors depend on the reconstructed mesh obtained by image segmentation and mesh processing. Moreover, CT image data were segmented semiautomatically; hence, observer dependence may taint the resulting segmentations. To this end (Afoke et al. 1980; Barr 1981; Lorensen and Cline 1987; Khan and Rayner 2003; Yushkevich et al. 2006; Anderson et al. 2008; Marusteri and Bacarea 2010; Allen et al. 2010; Harris et al. 2012, 2012; Ghasemi and Saleh 2012; Stoddard et al. 2017; Cooper et al. 2017) have performed research on reconstruction reproducibility and quantified geometric errors associated with 3D reconstruction. In particular (Harris et al. (2012) provided the community with reliable estimates of the systematic error induced by 3D reconstruction from volume data (<0.5 mm). Such errors are lower than the computed RMS errors. This study also reported that the distribution of error throughout the articulating surface is locally consistent and varies smoothly.

Towards the contribution of exponentiation to joint morphology, the exponent values of SE, SEB, TSEB, and SO did not differ greatly from the quadratic surfaces from which they originate. Given that the upper boundary set for these parameters was 4, to accommodate the approximation of the articular surfaces to quadrics, the fact that the maximum value observed for the supraquadratic exponents remained this close to its lower boundary leads to the conclusion that the interval was well set and that a quadratic-to-quartic exponent interval is enough to achieve good fitting results.

Concerning conicity, because of the more sphere-like appearance of the femoral head, the asphericity of the optimally adjusted surfaces in these cases is more difficult to identify by the naked eye than for acetabular articular surfaces. The geometric

properties which endow asphericity and higher geometric modeling freedom to the shape models originating from morphing transformations applied to the sphere are not clearly pronounced, for instance, in the set of surfaces represented in (Figure 2), even though the non-spherical primitives allow for a better fit to the femoral head point cloud, as demonstrated by the higher number of greyscale points in these surfaces' adjustments (Figure 3).

Unlike the femoral cases, the differences between the geometric features of shape are more easily distinguishable when acetabular point clouds are adjusted. As the fitting proceeds to more non-spherical shapes, the approximation of the point clouds improves drastically, especially when we move closer to the acetabular rim. Although visual inspection of the optimally fitted surfaces depicted in (Figure 4), particularly in the cases of sphere, rotational ellipsoid, and rotational conchoid, might suggest that the points located on the outer edge of the acetabulum are, in fact, exterior to the surface adjusted to them, the colour code used to discriminate points based on their Euclidean distance to the fitted surface clearly indicates that that is not the case. Given that points are coloured based on the same criteria described for the femoral case, points closer to the acetabular rim are, in truth, positioned below the surface, distanced more than 1.0 mm from it. The illusion that these points are located above the surface arises from the fact that the acetabular cavity is more planar than the femoral head. Therefore, surfaces with more pronounced curvatures overlap with the point cloud, as observable in the areas seemingly absent of points corresponding to the approximation of the sphere, rotational ellipsoid, ellipsoid, superellipsoid, and rotational conchoid. This higher level of asphericity inherent to the acetabular cavity is supported by the more straightforwardly identifiable geometric differences between all shape models. Such differences are particularly notable in ovoidal, superovoidal, and tapered ellipsoidal shapes.

There are a few limitations to the methodology presented in this work whose understanding can motivate future developments and improvements. First, it is necessary to take into account that bone-cartilage interface is not clearly delimited in CT images (Xi et al. 2003), increasing the difficulty in identifying the true contour of the articular surfaces of the hip joint and extracting the relevant anatomical and geometrical data which should be used in the surface-fitting framework. Even so, the surface-fitting errors indicate that the bone-cartilage boundary of the femoral heads and acetabular cavities closely resembled the idealised geometric primitives, as the error metrics were very small (i.e. on the order of 10–1 mm). As shape fitting only considered points from the bone-cartilage boundary, the shape fitting reflects a pure bony structure, which itself does not reflect the true articulation since the cartilage thickness is not uniform. By not taking into account the free surface of the articular surface, we eliminate any confounding effects from the cartilage. However, to assess the true articular shape, we should rely on MRI since it allows for mapping of the cartilage geometry, whereas CT does not allow this. We consider this as future work, since it would be interesting to assess if there is a correlation between cartilaginous surface and bony surface, namely, if cartilage thickness compensates the lack of bony asphericity or simply follows the underlying bony shape, and if this hypothetical correlation is verified for both healthy and unhealthy hips.

Secondly, this work lacks a biomechanical contribution *per se*, besides alerting the community that more representative shapes than the sphere may better describe hip biomechanics as ‘*form follows function*’. Although more work is required to achieve biomechanical relevance (e.g. hip joint simulations through finite-element analysis, Multibody or Discrete Element Analysis), we consider that this work does lay ground for further biomechanical research as the reported morphological findings may serve to inspire new hip prosthetic shapes. New shapes may even elucidate the effects of hip joint morphology on predictions of cartilage contact mechanics from a validated, subject-specific finite-element model of the human hip.

Thirdly, although we did not consider pathological hips, the clinical relevance of our study consists of introducing new shapes that define morphological parameters from CT scans. Note that, understanding the subjacent morphological features of a normal, asymptomatic hip joint is the first step in identifying abnormal and potentially pathological morphologies, such as the ones characterising femoroacetabular impingement and hip dysplasia. Our findings are relevant when compared to radiographic measurements which have been reported do not properly characterise the fémur and acetabulum, raising concerns on defining hip disorders and anatomy based on radiographic measurements alone (Clohisy et al. 2008; Jamali et al. 2013; Haldane et al. 2017). It is possible that clinicians are not only overdiagnosing and overtreating hip conditions but paradoxically missing the diagnosis entirely. Therefore, we consider that this study opens new research lines for clinical relevance as more representative shapes propose new metrics that unambiguously characterise femoral head and acetabular cavity geometries.

Finally, a Statistical Shape Modelling (SSM) approach based on Principal Component Analysis (PCA) would be necessary to better differentiate anatomical variations in the hip, thus, providing more useful insights into shape variation across the population. SSM data could be used to identify more differentiated or even novel shape variations between groups, which could, in turn, be used to develop more sensitive and specific clinical measurements. Besides comparing variations between male and female subjects, SSM could accurately describe, reproduce, quantify variation and compare morphologic differences between asymptomatic and symptomatic bone shapes. However, additional research on SSM as a clinical tool is required. Although a PCA-based statistical shape analysis is out of the scope of the presented work, we consider this topic to be a very interesting future work.

Notes

1. <https://mrl.sci.utah.edu/software/normal-hip-image-data/>.
2. www.itknap.org/.
3. www.paraview.org/.
4. <https://www.blender.org/>.

Acknowledgments

All authors are thankful for the financial support given by Portuguese Foundation for Science and Technology through national funds with references UID/CEC/50021/2019 and STREACKER UTAP-EXPL/CA/0065/2017.

Disclosure statement

No potential conflict of interest was reported by the authors.

Ethical approval

The data sets used in our study resulted from the approval by the Ethics Research Committee of the Nova Medical School | Faculdade de Ciências Médicas da Universidade Nova de Lisboa (CEFCM) under the Project entitled ‘DEFORMIDADES COXO-FEMURAIAS E CONFLITO FEMUROACE TABULAR: contributo epidemiológico, diagnóstico e prognóstico’ with reference nr.61/2014/CEFCM, and also by the University of Utah Institutional Review Board #10983.

Funding

This work was supported by the Fundação para a Ciência e a Tecnologia [UID/CEC/50021/2019,UTAP-EXPL/CA/0065/2017].

ORCID

Daniel Simões Lopes  <http://orcid.org/0000-0003-0917-9396>
 Vasco V. Mascarenhas  <http://orcid.org/0000-0002-5451-5021>
 Joaquim A. Jorge  <http://orcid.org/0000-0001-5441-4637>

References

- Afoke NY, Byers PD, Hutton WC. 1980. The incongruous hip joint. A casting study. *Bone Joint J.* 62(4):511–514.
- Ahn SJ. 2004. Least squares orthogonal distance fitting of curves and surfaces in space, series: lecture notes in computer science. Vol. 3151. USA: Springer.
- Allen BC, Peters CL, Brown NA, Anderson AE. 2010. Acetabular cartilage thickness: accuracy of three-dimensional reconstructions from multidetector CT arthrograms in a cadaver study. *Radiology.* 255:544–552. [PubMed: 20413764].
- Anderson AE, Ellis BJ, Maas SA, Weiss JA. 2010. Effects of idealized joint geometry on finite element predictions of cartilage contact stresses in the hip. *J Biomech.* 43(7):1351–1357.
- Anderson AE, Ellis BJ, Peters CL, Weiss JA. 2008. Cartilage thickness: factors influencing multidetector CT measurements in a phantom study. *Radiology.* 246:133–141. [PubMed: 18096534].
- Barr AH. 1981. Superquadrics and angle-preserving transformations. *IEEE Comput Graph Appl.* 1(1):11–23.
- Bazaraa MS, Sherali HD, Shetty CM. 1993. *Nonlinear programming: theory and algorithms.* Hoboken (NJ): Wiley.
- Berryman F, Pynsent P, McBryde C. 2014. A semi-automated method for measuring femoral shape to derive version and its comparison with existing methods. *Int J Numer Methods Biomed Eng.* 30:1314–1325. doi:10.1002/cnm.2659.
- Carter TC. 1968. The hen’s egg: a mathematical model with three parameters. *Br Poult Sci.* 9(2):165–171.
- Cerveri P, Manzotti A, Baroni G. 2014. Patient-specific acetabular shape modeling: comparison among sphere, ellipsoid and conchoid parameterisations. *Comput Methods Biomech Biomed Engin.* 17(5):560–567.
- Cerveri P, Marchente M, Chemello C, Confalonieri N, Manzotti A, Baroni G. 2011. Advanced computational framework for the automatic analysis of the acetabular morphology from the pelvic bone surface for hip arthroplasty applications. *Ann Biomed Eng.* 39(11):2791–2806.
- Clohisy JC, Carlisle JC, Trousdale R, Kim Y-J, Beaulé PE, Morgan P, Steger-May K, Schoenecker PL, Millis M. 2008. Radiographic evaluation of the hip has limited reliability. *Clin Orthop Relat Res.* 467:666–675. doi:10.1007/s11999-008-0626-4.
- Cooper RJ, Mengoni M, Groves D, Williams S, Bankes MJ, Robinson P, Jones AC. 2017. Three-dimensional assessment of impingement risk in geometrically parameterised hips compared with clinical measures. *Int J Numer Methods Biomed Eng.* 33:e2867. doi:10.1002/cnm.2867.

- Ghasemi A, Saleh Z. 2012. Normality tests for statistical analysis: a guide for non-statisticians. *Int J Endocrinol Metab.* 10(2):486–489.
- Gu D, Chen Y, Dai K, Zhang S, Yuan J. 2008. The shape of the acetabular cartilage surface: A geometric morphometric study using three-dimensional scanning. *Med Eng Phys.* 30(8):1024–1031.
- Gu DY, Dai KR, Hu F, Chen YZ. 2010. The shape of the acetabular cartilage surface and its role in hip joint contact stress. 2010 Annual International Conference of the IEEE Engineering in Medicine and Biology; Buenos Aires, Argentina. IEEE. p. 3934–3937.
- Gu DY, Hu F, Wei JH, Dai KR, Chen YZ. 2011. Contributions of non-spherical hip joint cartilage surface to hip joint contact stress. 2011 Annual International Conference of the IEEE Engineering in Medicine and Biology Society; Boston, MA. IEEE. p. 8166–8169.
- Haldane CE, Ekhtiari S, de SA D, Simunovic N, Ayeni OR. 2017. Preoperative physical examination and imaging of femoroacetabular impingement prior to hip arthroscopy—a systematic review. *J Hip Preserv Surg.* 1–13. doi:10.1093/jhps/hnx020.
- Harris MD, Anderson AE, Henak CR, Ellis BJ, Peters CL, Weiss JA. 2012. Finite element prediction of cartilage contact stresses in normal human hips. *J Orthop Res.* 30(7):1133–1139. doi:10.1002/jor.22040.
- Jamali AA, Mak W, Wang P, Tai L, Meehan JP, Lamba R. 2013. What is normal femoral head/neck anatomy? An analysis of radial CT reconstructions in adolescents. *Clin Orthop Relat Res.* 471:3581–3587. doi:10.1007/s11999-013-3166-5.
- Jiang HB, Liu HT, Han SY, Fen LIU. 2010. Biomechanics characteristics of new type artificial hip joint. *Adv Nat Sci.* 3(2):258–262.
- Kang M. 2004. Hip joint center location by fitting conchoid shape to the acetabular rim region of MR images. *Engineering in Medicine and Biology Society, 2004. IEMBS'04. 26th Annual International Conference of the IEEE; Vol. 2; San Francisco, CA. IEEE.* p. 4477–4480.
- Kang MJ, Sadri H, Stern R, Magnenat-Thalmann N, Hoffmeyer P, Ji HS. 2010. Determining the location of hip joint centre: application of a conchoid's shape to the acetabular cartilage surface of magnetic resonance images. *Comput Methods Biomech Biomed Engin.* 14(1):65–71.
- Khan A, Rayner GD. 2003. Robustness to non-normality of common tests for the many-sample location problem. *J Appl Math Decis Sci.* 7(4):187–206. doi:10.1155/S1173912603000178.
- Liu B, Hua S, Zhang H, Liu Z, Zhao X, Zhang B, Yue Z. 2014. A personalized ellipsoid modeling method and matching error analysis for the artificial femoral head design. *Comput-Aided Des.* 56:88–103.
- Liu B, Zhang H, Hua S, Jiang Q, Huang R, Liu W, Yue Z, Zhang B, Yue Z. 2015. An automatic segmentation system of acetabulum in sequential CT images for the personalized artificial femoral head design. *Comput Methods Programs Biomed.* 127:318–335.
- Lopes DS, Pires SM, Mascarenhas VV, Silva MT, Jorge JA. 2018 September. On a “Columbus’ egg”: modeling the shape of asymptomatic, dysplastic and impinged hip joints. *Med Eng Phys.* 59:50–55. doi:10.1016/j.medengphy.2018.07.001.
- Lopes DS, Neptune RR, Gonçalves AA, Ambrósio JA, Silva MT. 2015. Shape analysis of the femoral head: a comparative study between spherical,(super) ellipsoidal, and (super) ovoidal shapes. *J Biomech Eng.* 137(11):114504.
- Lorensen WE, Cline HE. 1987. Marching cubes: A high resolution 3D surface construction algorithm. *ACM SIGGRAPH Comp Graph.* 21:163–169.
- MacConaill MA. 1966. The geometry and algebra of articular kinematics. *Biomed Eng.* 1:205–212.
- MacConaill MA. 1973. A structuro-functional classification of synovial articular units. *Ir J Med Sci.* 142(1):19–26.
- Marusteri M, Bacarea V. 2010. Comparing groups for statistical differences: how to choose the right statistical test? *Biochemia Med.* 20(1):15–32. [Accessed 2019 Mar 4]. <https://hrcak.srce.hr/47847>.
- Menschik F. 1997. The hip joint as a conchoid shape. *J Biomech.* 30(9):971–973.
- Paganelli CV, Olszowka A, Ar A. 1974. The avian egg: surface area, volume, and density. *Condor.* 76(3):319–325.
- Rouvière H, Delmas A, Götzens García V, Testut JL, Jacob R, Velayos JLS, Testut OL. 2005. *Anatomía humana: descriptiva, topográfica y funcional* (No. 611). Barcelona (Spain): Masson.
- Standring S, Ed. 2015. *Gray's anatomy: the anatomical basis of clinical practice.* London (UK): Elsevier Health Sciences.
- Stoddard MC, Yong EH, Akkaynak D, Catherine Sheard JA, Mahadevan TL. 2017 Jun 23. Avian egg shape: form, function, and evolution, science. p. 1249–1254.
- Subburaj K, Ravi B, Agarwal M. 2010 June. Computer-aided methods for assessing lower limb deformities in orthopaedic surgery planning. *Comput Med Imaging Graphics.* 34(4):277–288. doi:10.1016/j.compmedimag.2009.11.003.
- Todd PH, Smart IH. 1984. The shape of birds’ eggs. *J Theor Biol.* 106(2):239–243.
- Vesalius A. 1998. *De humani corporis fabrica* (No. 4). Novato (CA): Norman Publishing.
- Williams GM, Chan EF, Temple-Wong MM, Bae WC, Masuda K, Bugbee WD, Sah RL. 2010. Shape, loading, and motion in the bioengineering design, fabrication, and testing of personalized synovial joints. *J Biomech.* 43(1):156–165.
- Wu HH, Wang D, Ma AB, Gu DY. 2016. Hip joint geometry effects on cartilage contact stresses during a gait cycle. *IEEE 38th Annual International Conference of the Engineering in Medicine and Biology Society (EMBC); Orlando, FL.* p. 6038–6041.
- Xi J, Hu X, Jin Y. 2003. Shape analysis and parameterized modeling of hip joint. *J Comput Inf Sci Eng.* 3(3):260–265.
- Yushkevich PA, Piven J, Hazlett HC, Smith RG, Ho S, Gee JC, Gerig G. 2006. User-guided 3D active contour segmentation of anatomical structures: significantly improved efficiency and reliability. *Neuroimage.* 31(3):1116–1128.